Available online at www.sciencedirect.com
SCIENCE DIRECT
ELSEVIER
Journal of the European Ceramic Society 26 (2006) 1149–1158
ECERS
www.elsevier.com/locate/jeurceramsoc

Microstructural characterization and crystallization behaviour of $(1-x)TeO_2$–xWO_3 ($x = 0.15$, 0.25, 0.3 mol) glasses

M.L. Öveçoğlu [a,*], G. Özen [b], S. Cenk [c]

[a] *Department of Metallurgical and Materials Engineering, Faculty of Chemical and Metallurgical Engineering, Istanbul Technical University, Maslak 34469, Istanbul, Turkey*
[b] *Department of Physics, Faculty of Science and Letters, Istanbul Technical University, Maslak 34469, Istanbul, Turkey*
[c] *TUBITAK, The National Research Institute of Electronics, Gebze 41470, Kocaeli, Turkey*

Received 25 August 2004; received in revised form 5 January 2005; accepted 10 January 2005
Available online 12 March 2005

Abstract

DTA, XRD and SEM investigations were conducted on the $(1-x)TeO_2$–xWO_3 glasses (where $x = 0.15$, 0.25 and 0.3). Whereas the $0.75TeO_2$–$0.25WO_3$ and $0.7TeO_2$–$0.3WO_3$ glasses show no exothermic peaks, an indication of no crystallization in their glassy matrices, two crystallization peaks were observed on the DTA plot of the $0.85TeO_2$–$0.15WO_3$ glass. On the basis of the XRD measurements of the $0.85TeO_2$–$0.15WO_3$ glass samples heated to 510 °C and 550 °C (above the peak crystallization temperatures), α-TeO_2 (paratellurite), γ-TeO_2 and WO_3 phases were detected in the sample heated to 510 °C and the α-TeO_2 and WO_3 phases were present in the sample heated to 550 °C. SEM micrographs taken from the $0.85TeO_2$–$0.15WO_3$ glass heated to 510 °C showed that centrosymmetrical crystals were formed as a result of surface crystallization and were between 3 μm and 15 μm in width and 12 μm and 30 μm in length. On the other hand, SEM investigations of the $0.85TeO_2$–$0.15WO_3$ glass heated to 550 °C revealed the evidence of bulk massive crystallization resulting in lamellar crystals between 1 μm and 3 μm in width and 5 μm and 30 μm in length. DTA analyses were carried out at different heating rates and the Avrami constants for the $0.85TeO_2$–$0.15WO_3$ glass heated to 510 °C and 550 °C were calculated as 1.2 and 3.9, respectively. Using the modified Kissinger equation, activation energies for crystallization were determined as 265.5 kJ/mol and 258.6 kJ/mol for the $0.85TeO_2$–$0.15WO_3$ glass heated to 510 °C and 550 °C, respectively.

Keywords: Crystallization; Glasses; TeO_2; WO_3; Microstructure-final

1. Introduction

The tellurite glasses when doped with rare earth ions have great advantages over the crystalline systems since they can be easily prepared in a large variety of chemical compositions with high optical quality. Recently, the interest has grown in the conversion of infrared into visible light by energy up-conversion, due to the potential applications in photonics such as optical data storage, lasers, sensors and optical displays.[1] Tellurium oxide (TeO_2)-based glasses containing heavy metal oxides such as Tl_2O, Bi_2O_3 and WO_3 are especially potential candidates for optoelectronic devices due to their superior physical properties such as low melting temperature, high dielectric constant, high refractive index, large third order non-linear susceptibility, good infrared transmissivity and relatively high chemical durability and high electrical conductivity.[2] In these glasses, TeO_2 is the main glass former which does not transform to the glassy state under normal conditions. The addition of alkali oxide to tellurites increases their glass forming tendency and produces non-bridging oxygen sites which reduces the average coordination number.[3]

Currently there exists a substantial amount of literature which has reported the thermal, optical and structural properties of TeO_2 based glasses.[4–8] Kosuge et al.[9] reported that the R_2O–TeO_2–WO_3 (R: Li, Na, and K) glass systems have a very wide glass forming region suggesting that

* Corresponding author. Tel.: +90 212 285 3355; fax: +90 212 285 2925.
E-mail address: ovecoglu@itu.edu.tr (M.L. Öveçoğlu).

0955-2219/$ – see front matter © 2005 Elsevier Ltd. All rights reserved.
doi:10.1016/j.jeurceramsoc.2005.01.039

the R_2O–TeO_2–WO_3 glasses are suitable for the study of the structural behavior of TeO_2 containing glasses.[10] Blanchandin et al.[11] have investigated the structure of TeO_2–WO_3 glasses using DSC and XRD techniques. They reported two new metastable crystalline phases in these glasses. However, the data available on the crystallization kinetics, microstructural morphology and formation of crystalline phases in the TeO_2–WO_3 system, to our knowledge, are incomplete. The present study aims to fulfil this task. The present study is also part of an ongoing investigation on the effect of the WO_3 content on the microstructure and crystallization kinetics of $(1-x)TeO_2$–xO_3 glasses and on the spontaneous emission probabilities of the doped thulium (Tm) ion in these glasses.[12,13] In this work, $(1-x)TeO_2$–xO_3 glasses (where $x = 0.15$, 0.25 and 0.3 in molar ratio) were investigated by means of DTA, X-ray diffractometry and SEM techniques.

2. Experimental procedure

Tellurite glasses were prepared with the compositions of $(1-x)TeO_2 + xWO_3$ ($x = 0.15$, 0.25, 0.30 in molar ratio), all doped with 1.0 mol% Tm_2O_3 (now hereafter referred to as the $0.85TeO_2$–$0.15WO_3$, $0.75TeO_2$–$0.25WO_3$ and $0.70TeO_2$–$0.30WO_3$ glasses, respectively). The Tm ion is doped to exhibit absorption and luminescence transitions in the TeO_2–WO_3 glasses intended for solid state laser applications. All chemicals used in this study were reagent grade of TeO_2 (99.999 % purity, Aldrich Chemical Company), WO_3 (99.99% purity, Merck Chemical Company), and Tm_2O_3 (99.9% purity Sigma Chemical Company). Batches of 7 g size were thoroughly mixed and melted in a platinum crucible at 950 °C for 30 min in an electrically heated furnace in air, followed by removing the glass melts from the furnace and quenching them in air by casting and pressing between two rectangular graphite slabs at room temperature. A series of wet chemistry analyses were done on bulk as-quenched and heat-treated TeO_2–WO_3 samples. These analyses have shown that the initial elemental stoichiometry of the bulk glass samples did not change after quenching and heat-treating.

Differential thermal analysis scans of as-cast glass specimens were carried out in a Rigaku Thermoflex Thermal Analyzer equipped with PTC-10A temperature control unit in order to determine the characteristic glass transition temperatures (T_g) and the peak crystallization temperatures (T_p). After pulverizing and grinding as-cast glass, static non-isothermal DTA experiments were performed by heating 20 mg glass powder at heating rates of 5 °C/min, 10 °C/min, 15 °C/min and 20 °C/min in a Pt-crucible and using the same amount of Al_2O_3 as the reference material in the temperature range between 20 °C and 700 °C. The crucibles used were matched pairs made of platinum and the temperature precision was ±1 °C. The T_g temperature is selected as the inflection point of the step change of the calorimetric signal,[11] whereas the T_c temperature is measured at the onset of crystallization and the T_p temperature is measured at the peak of crystallization. Crystallization experiments of annealed glass samples were carried out in a muffle furnace which had an approximate heating rate of 10 °C/min.

The microstructural characterization of the as-cast and crystallized glass samples was carried out using both electron microscopy and X-ray diffraction techniques. Scanning electron microscopy (SEM) investigations were conducted in a JEOL™ Model JSM-T330 operated at 25 kV and linked with an energy dispersive (EDS) attachment. For the SEM investigations, optical mount specimens were prepared using standard metallographic techniques followed by chemical etching in a HF solution (5%) for 1.5 min. The etched optical samples were coated with carbon. The X-ray diffraction investigations were carried out in a Philips™ Model PW3710 using Cu Kα radiation at 40 kV and 40 mV settings in the 2θ range from 20° to 90°. The crystallized phases were identified by comparing the peak positions and intensities with those in the Joint Committee on Powder Diffraction Standards (JCPDS) data files.

3. Results and discussion

3.1. Thermal analysis and microstructural characterization

Differential thermal analysis (DTA) investigations were conducted on the as-cast TeO_2–WO_3 glasses. Preliminary DTA runs were carried out on the glasses containing no Tm_2O_3 (undoped) and on the ones doped with 1 mol% Tm_2O_3 (0.01 mol Tm_2O_3) and DTA curves were identical for the undoped and doped glass of a given composition. On the basis of these DTA runs, it can be concluded that the addition of 0.01 mol Tm_2O_3 has no effect on the thermal properties of the $(1-x)TeO_2$–xWO_3 glasses. Therefore, the experimental results presented in this investigation belong to those of the 0.01 mol Tm_2O_3 doped $(1-x)TeO_2$–xWO_3 glasses. Fig. 1a–c represents the respective DTA curves of the $0.85TeO_2$–$0.15WO_3$, $0.75TeO_2$–$0.25WO_3$ and $0.70TeO_2$–$0.30WO_3$ glasses scanned at a rate of 10 °C/min. As seen in Fig. 1, each DTA scan exhibits a small endothermic peak corresponding to the glass transition temperature, T_g. The T_g values, listed in Table 1, shift to higher values with increasing WO_3 content. The $0.75TeO_2$–$0.25WO_3$ and $0.7TeO_2$–$0.3WO_3$ glasses do not show any exothermic peaks, an indication of no crystallization in their glassy matrices. On the other hand, two exothermic peaks occurring at 496 °C and at 537 °C following the glass transition at 362 °C were observed for the $0.85TeO_2$–$0.15WO_3$ glass (Fig. 1a). Both peaks can be attributed to the formation and/or transformation of crystalline phases. The temperature difference between the T_g and the first exothermic peak, T_{p1}, $\Delta T = T_{p1} - T_g$, gives a measure for the thermal stability of the glass against crystallization. The ΔT value is 134 °C for the $0.85TeO_2$–$0.15WO_3$ glass and is higher than that of the

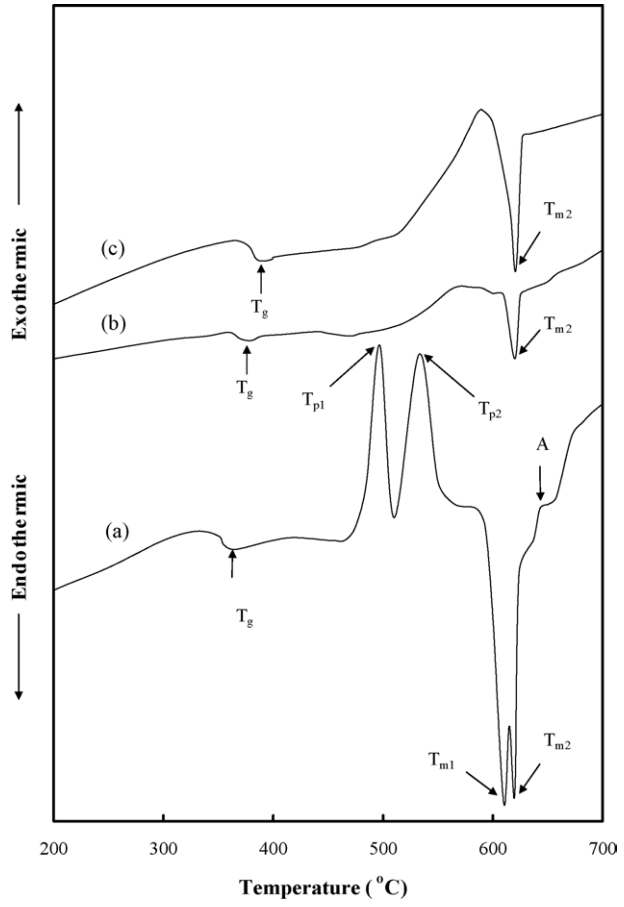

Fig. 1. DTA curves of $(1-x)TeO_2$–xO_3 glasses with (a) $x = 15$ mol%, (b) $x = 25$ mol% and (c) $x = 30$ mol%. All glasses contain 1.0 mol% Tm_2O_3. The curves were obtained with a heating rate 10 °C/min. T_g, T_p and T_m are the glass transition, the crystallization and melting temperatures, respectively.

$50TeO_2$–50LiCl glass.[7] All three glasses exhibit the same endothermic peak occurring at $T_{m2} = 622$ °C. In addition, the $0.85TeO_2$–$0.15WO_3$ glass shows a second endothermic peak at $T_{m1} = 607$ °C (Fig. 1a).

The nature of the endothermic peak occurring at $T_{m2} = 622$ °C for all glass compositions can be verified by consulting the TeO_2–WO_3 pseduo-binary phase diagram presented by Blanchandin et al.[11] who showed that the eutectic reaction: Liquid ↔ α-TeO_2 (paratellurite) + orthorhombic WO_3 takes place at 622 °C for the eutectic composition 22 ± 1 mol% WO_3. Therefore, the endothermic peak at $T = 622$ °C in Fig. 1 corresponds to the eutectic temperature of the TeO_2–WO_3 binary. Considering the $0.85TeO_2$–$0.15WO_3$ glass composition employed in the present investigation, about 63% of the α-TeO_2 and all WO_3 transform completely to liquid above the eutectic temperature. According to the phase diagram,[11] the remnant primary α-TeO_2 phase for the $0.85TeO_2$–$0.15WO_3$ glass melts at about $T = 656$ °C as indicated by point A in Fig. 1a. On the other hand, for the other compositions of the present study, viz. the $0.75TeO_2$–$0.25WO_3$ and $0.7TeO_2$–$0.3WO_3$ glasses, the α-TeO_2 phase melts completely at $T_{m2} = 622$ °C (Fig. 1b and c) and there is still remnant orthorhombic WO_3 phase above the eutectic temperature. As reported by Salje and Viswanathan,[14] the orthorhombic WO_3 phase transforms to the tetragonal WO_3 phase at $T = 740$ °C which is beyond the range of the present DTA investigation. The endothermic peak occurring at $T_{m1} = 607$ °C in Fig. 1a for the $0.85TeO_2$–$0.15WO_3$ glass can not be verified by the binary phase diagram suggesting that it could correspond to the melting reaction of a metastable phase.

On the basis of DTA results, X-ray diffractometry scans were carried out to verify the nature of crystallizing phase(s) in the glassy matrix at temperatures above T_g for all glasses of the present investigation. X-ray diffractometry patterns of the as-cast $(1-x)TeO_2$–xWO_3 ($x = 0.15$, 0.25, 0.3 mol) glasses revealed no detectable peaks, confirming that they consist of only amorphous glass matrix in the as-cast state. Further, conforming with the DTA data, X-ray patterns of the $0.75TeO_2$–$0.25WO_3$ and $0.7TeO_2$–$0.3WO_3$ glasses taken from specimens heated above T_g did not show any crystallization peaks. On the other hand, as seen in Fig. 2, X-ray investigations on the $0.85TeO_2$–$0.15WO_3$ glass heated to 510 °C and 550 °C above the peak crystallization temperature at a rate of 10 °C/min followed by quenching in air showed the evidence of devitrification. Fig. 2b shows the X-ray diffraction pattern of the $85TeO_2$–$15WO_3$ glass heated at a rate of 10 °C/min to 510 °C followed by quenching in air. The *d*-values of the first, fourth and fifth peaks in Fig. 2b matched the card values of the paratellurite (α-TeO_2) phase which has a tetragonal crystal structure with lattice parameters $a = 0.481$ nm and $c = 0.761$ nm.[15] On the other hand, the *d*-values of the second and third peaks matched the calculated values of the new polymorph named by Blanchandin et al.[11] as the γ-TeO_2 phase having the orthorhombic symmetry with the calculated lattice parameters $a = 0.845$ nm, $b = 0.499$ nm and $c = 0.430$ nm. Thus, it is evident from Fig. 2b that TeO_2 exists in two polymorphs at 510 °C: the stable α-TeO_2 phase and the metastable γ-TeO_2 phase. In addition, characteristic peaks belonging to

Table 1
Value of glass transition, T_g, crystallization peak temperature, T_p, and melting, T_m, temperatures of the $(1-x)TeO_2$–xWO_3 glasses

Glass composition (mol%)		T_g (°C)	T_{p1} (°C)	T_{p2} (°C)	T_{m1} (°C)	T_{m2} (°C)	$\Delta T = T_c - T_g$ (°C)
TeO_2	WO_3						
70	30	398	–	–	–	622	–
75	25	386	–	–	–	622	–
85	15	362	496	537	607	622	134

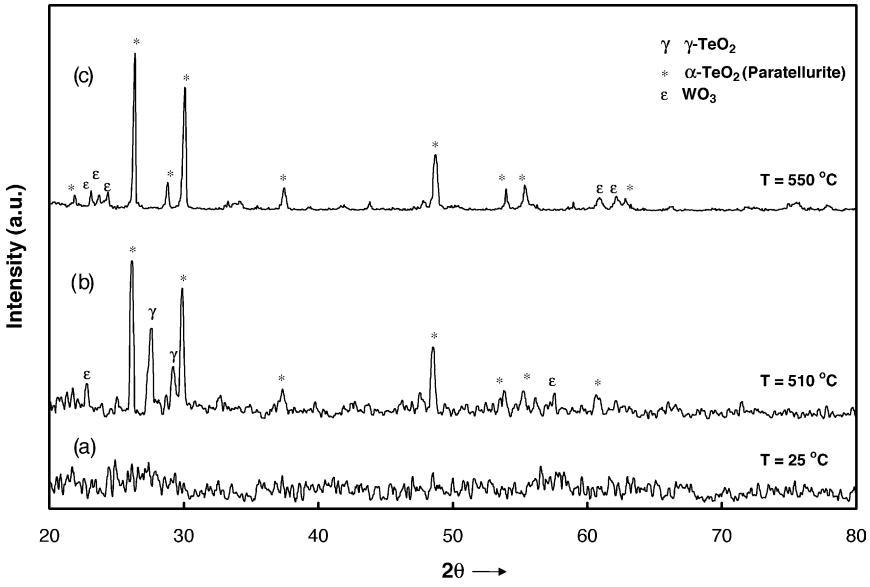

Fig. 2. X-ray diffraction patterns of the $85TeO_2$–$15WO_3$ glass taken (a) at room temperature, (b) heated at a rate of 10 °C/min to 510 °C and (c) heated at a rate of 10 °C/min to 550 °C followed by quenching in air.

WO_3 are also seen which has an orthorhombic crystal structure with lattice parameters $a = 0.738$ nm, $b = 0.751$ nm and $c = 0.385$ nm.[16] On the basis of Fig. 2b, it can be concluded that the first crystallization peak (exotherm at $T = 496$ °C) of the DTA scan of the $0.85TeO_2$–$0.15WO_3$ glass shown in Fig. 1a corresponds to the simultaneous crystallization of these polymorphs and WO_3. Fig. 2c shows the X-ray diffraction pattern of the $85TeO_2$–$15WO_3$ glass heated at a rate of 10 °C/min to 550 °C followed by quenching in air. In addition to the characteristic WO_3 peaks, other peaks in Fig. 2c matched the *d*-values of the paratellurite (α-TeO_2) phase and there is no evidence of the metastable γ-TeO_2 phase. Thus, on the basis of Fig. 2c, the second exotherm in Fig. 1a is the result of the transformation γ-TeO_2 → α-TeO_2. The DTA (Fig. 1a) and XRD results (Fig. 2b and c) for the $0.85TeO_2$–$0.15WO_3$ glass of the present investigation partially match the results of Blanchandin et al.[11] who reported three peaks on DSC curves, first corresponding to the crystallization of γ-TeO_2, second to the crystallization of WO_3 and the third peak pertaining to the transformation γ-TeO_2 → α-TeO_2. In other words, despite the fact that the same crystalline phases are found in both investigations, their order of appearance in a thermal plot is distinct in the study by Blanchandin et al.[11] compared to the present study whose first thermal peak incorporates the crystallization of the above-mentioned phases. We believe that this discrepancy is due to higher T_g and higher thermal stability value ($\Delta T = 134$ °C) achieved in the present study.

To obtain better understanding of the morphology and size of the crystallizing phases, SEM investigations were conducted on the $0.85TeO_2$–$0.15WO_3$ glass heated to 510 °C and to 550 °C followed by air-quenching. Fig. 3a–d shows a series of SEM micrographs taken from the outer surface and Fig. 3e shows the SEM micrograph taken from the cross-section of the $0.85TeO_2$–$0.15WO_3$ sample heated to $T = 510$ °C followed by quenching in air. Fig. 3a is a representative SEM/SEI micrograph (secondary electron imaging mode) which reveals the presence of large centrosymmetric fan-like crystals varying between 3 μm and 15 μm in width and about 12 μm and 30 μm in length. EDS spectra taken from four different locations on these crystals (region *T* in Fig. 3a) have shown that they contained 35.36 ± 1.3 at.% Te, 4.53 ± 0.3 at.% W, 50.11 ± 0.2 at% O, indicating that these are TeO_2-rich crystals surrounded by a glassy matrix (region G). In addition, white globular particles (indexed as W) varying between 3 μm and 4 μm in size are also present in the microstructure. EDS spectra taken from these globular particles revealed that they contained 28.24 ± 1.5 at.% W, 69.11 ± 0.2 at.% O, 2.45 ± 1.3 at.% Te, suggesting that they are the WO_3-rich crystals. Fig. 3b and c shows the SEM micrographs from a different location taken in the secondary (SEI), back-scatterred (BEI) electron imaging modes, respectively, and Fig. 3d is the corresponding X-ray topography micrograph. Fig. 3b–d suggests that these crystals have penetration depths (thickness) of only few microns into the glassy matrix. Fig. 3e is a cross-sectional SEM/SEI micrograph taken at a tilt angle of 75° from the same region which reveals a worm-like structure typical of an amorphous glass matrix. Thus, as can also be seen in Fig. 3e, the TeO_2-rich crystals do not penetrate into the bulk of the glass matrix which indicates the fact that surface crystallization is the predominant mechanism for the $0.85TeO_2$–$0.15WO_3$ sample heated to $T = 510$ °C. EDS spectra taken from four different locations of the sample cross-section (region G in Fig. 3e) revealed that the amorphous glass matrix in the bulk of the sample contained 26.10 ± 0.5 at.% Te, 13.73 ± 0.3 at.% W and 60.16 ± 0.3 at.% O. Fig. 4a–c shows the respective SEM micrographs taken from the surface of the $85TeO_2$–$15WO_3$ sample heated to 550 °C which reveal lamellar crystals in the

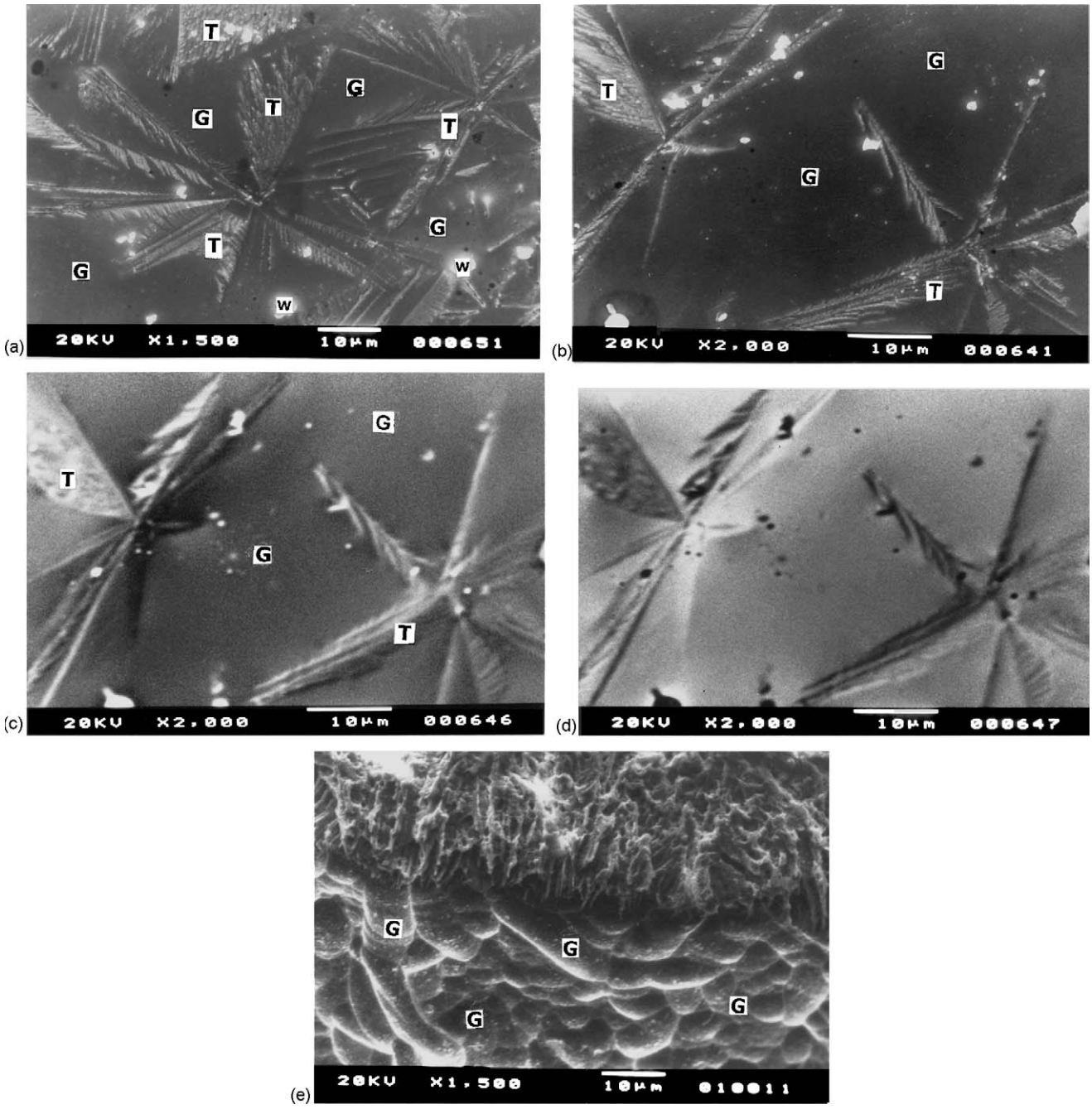

Fig. 3. SEM micrographs of the $85TeO_2$–$15WO_3$ glass heated at a rate of 10 °C/min to 510 °C followed by quenching in air: (a) a representative SEM/SEI micrograph showing the morphology of fan-like surface crystals, (b) SEM/SEI, (c) SEM/BEI and (d) topography micrographs taken from a region indicating the shallow nature of these crystals, (e) a cross-sectional SEM micrograph indicating the presence of typical amorphous (glassy) worm structure.

shape of long rods between 1 μm and 2 μm in thickness and 5 μm and 30 μm in length oriented in various directions. Furthermore, these micrographs reveal the fact that massive crystallization must have taken place in the microstructure. EDS analyses taken from these crystals revealed that they contained 34.7 ± 1.2 at.% Te, 3.65 ± 0.7 at.% W, 52.6 ± 0.9 at.% O, suggesting that they are TeO_2-rich crystals. Fig. 4d is a cross-sectional SEM micrograph which shows that these crystal rods penetrated into the bulk of the sample in various directions. EDS spectra taken from different regions in the crystals (regions Y in Fig. 4d) have confirmed that these are the TeO_2-rich crystals seen in Fig. 4a–c.

3.2. Activation energy determination

Fig. 5 shows the DTA thermograms of the as-cast $0.85TeO_2$–$0.15WO_3$ glass scanned at the heating rates of 5 °C/min, 10 °C/min, 15 °C/min and 20 °C/min. The glass-

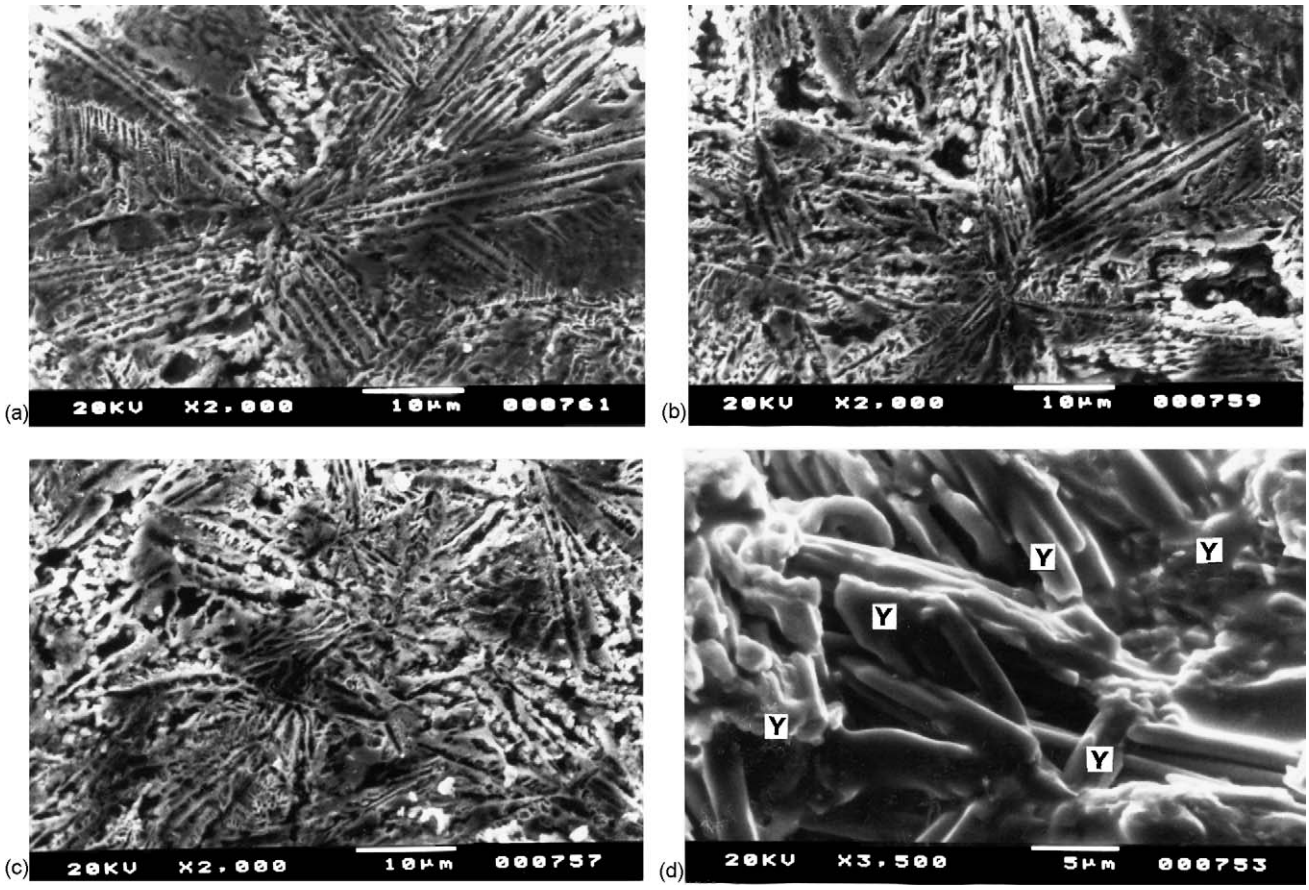

Fig. 4. (a–c) SEM micrographs and (d) cross-sectional SEM micrographs of the $85TeO_2$–$15WO_3$ glass heated at a rate of 10 °C/min to 550 °C followed by quenching in air.

transition (T_g), and the peak crystallization temperatures (T_{p1} and T_{p2}) are listed in Table 2. As seen in Table 2, the faster the heating rates, the higher the peak temperatures and larger the peak heights become. Similar to other thermal analysis investigations reported in the literature,[17–19] the T_g and T_p temperatures shift to higher values with increasing heating rate. The shift of peak temperatures with different DTA heating rates can be used to estimate the activation energy for crystallization and the governing crystallization mechanism. If the nucleation and crystallization growth processes take place simultaneously during the DTA runs, the activation energy for the crystallization of the glass samples is determined

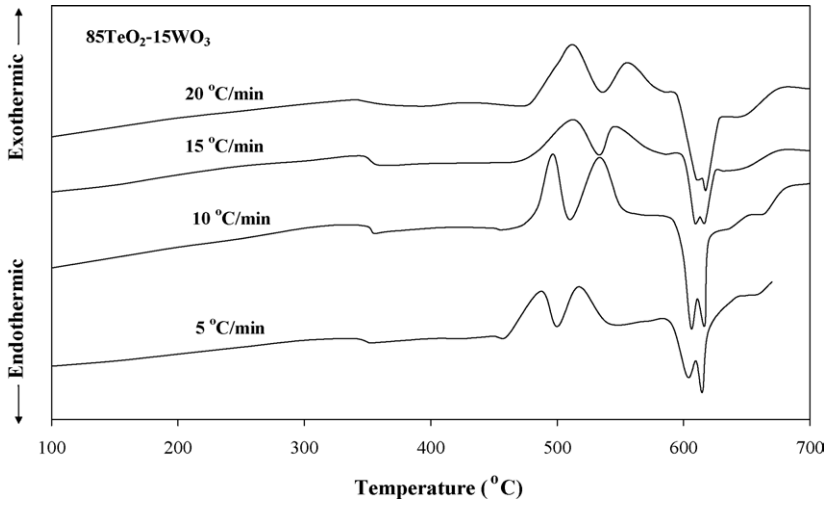

Fig. 5. DTA curves of the $85TeO_2$–$15WO_3$ glasses scanned at heating rates of 5, 10, 15, 20 °C/min.

Table 2
Heating rate, glass transition and peak crystallization temperatures of the $85TeO_2 + 15WO_3$ sample detected during the DTA scans

B (°C/min)	T_g (°C)	T_{p1} (°C)	T_{p2} (°C)
5	361	487	517
10	359	497	533
15	355	507	545
20	352	514	555

by using the modified Kissinger method as shown by Matusita et al.[20–22] The crystallization peak temperature is obtained as a function of the heating rate, then the following relationship is applied:

$$\ln\left(\frac{B^n}{T_p^2}\right) = -\left(\frac{mQ}{RT_p}\right) + K \quad (1)$$

where B is the heating rate, T_p is the peak crystallization temperature for a given B, Q is the activation energy for crystallization, R is the gas constant, n is the Avrami parameter, m is the dimensionality of crystal growth and K is constant. As listed in detail in Table 3, the parameters n and m are characteristics of various crystallization mechanisms and they can take on various values depending on the governing crystallization mechanism; $m = 1$ when the predominant mechanism is surface crystallization and $m = 3$ for bulk crystallization.[20,21,23] When nucleation takes place during DTA, $m = n - 1$. For the special case where surface crystallization is the predominant mechanism, $n = m = 1$ for all heating rates, then Eq. (1) reduces to the well-known Kissinger equation.[24]

The value of the Avrami constant, n, can be determined from the Ozawa equation[25]:

$$\left|\frac{\mathrm{d}\ \ln(-\ln(1-x))}{\mathrm{d}\ \ln B}\right|_T = -n \quad (2)$$

where x is the volume fraction crystallized at a fixed temperature T for the heating rate of B. x is the ratio of the partial area

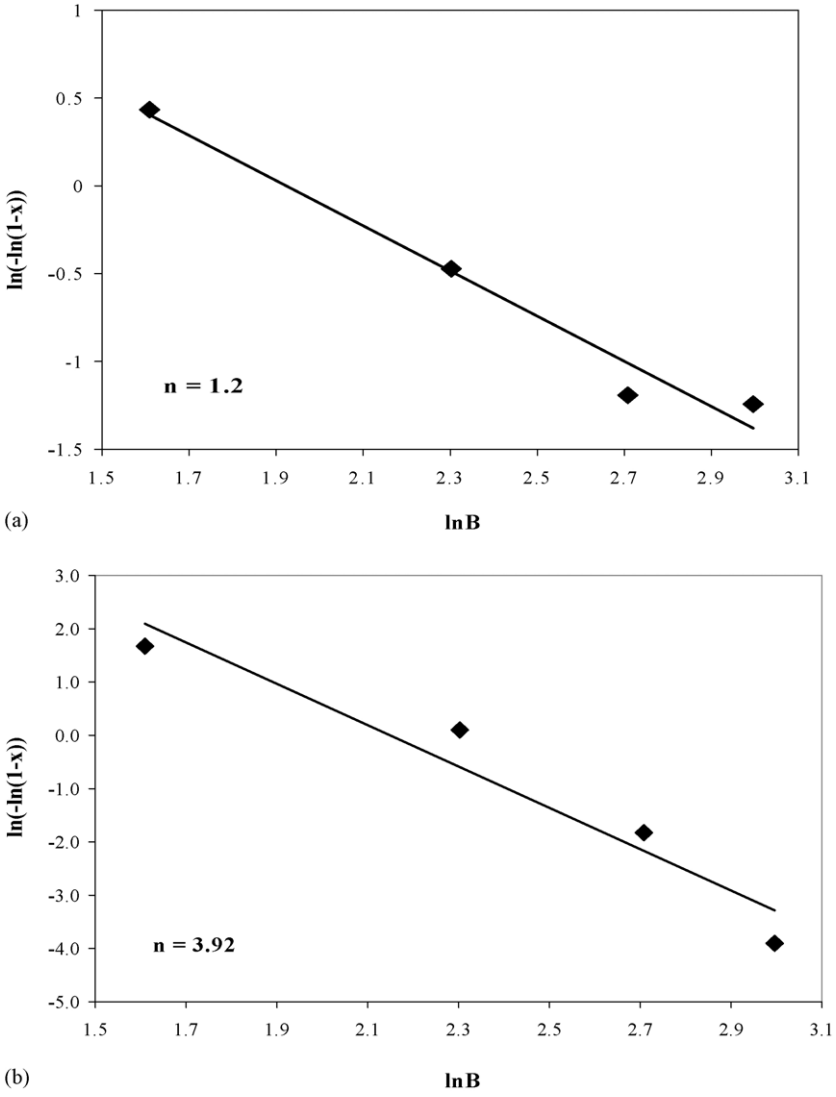

Fig. 6. (a) The Ozawa plot associated with the first exotherm (T_{p1}) of the $85TeO_2$–$15WO_3$ glass shown in Fig. 5.

at a given temperature, T, to the total area under the crystallization exotherm and its value can be determined from the exotherms seen in Fig. 5. The plot of $\ln(-\ln(1-x))$ versus $\ln B$ should be a straight line whose slope is n.

Fig. 6a and b represents the respective Ozawa[25] plots ($\ln(-\ln(1-x))$ versus $\ln B$) of the $0.85TeO_2$–$0.15WO_3$ sample related to the first and second exothermic peak shown in Fig. 5. The values of n determined from the slopes of these plots are 1.2 for the first exothermic peak (Fig. 6a) and 4.01 for the second exotherm (Fig. 6b). Considering experimental errors, these values can be taken as $n = 1$ for the first exotherm[23] and $n = 4$ for the second exotherm. Thus, as listed in Table 3, the m value associated with the first exotherm is $m = n = 1$ for the special case of surface crystallization and it is equal to $n - 1 = 3$ for the second exotherm. These values indicate that surface crystallization is associated with the first exotherm and bulk crystallization is dominant following the second exotherm in Fig. 5. Once n and m values are known, Eq. (1) can be used to calculate the activation energy for crystallization. A plot of $\ln(B^n/T_p^2)$ versus $1/T_p$ should yield a straight line whose slope ($-mQ/R$) can be used to calculate the activation energy for crystallization, Q.[19] In other words, by substituting the appropriate values of n, m and R (8.3144 J/mol K) in Eq. (1) for these peaks, the activation energies are found from the slope ($-mQ/R$) of a plot of $\ln(B^n/T_p^2)$ against $1/T_p$. Fig. 7a and b gives the graphical solutions of Eq. (1) showing the modified Kissinger plots of $\ln(B^n/T_p^2)$ versus $1/T_p$ pertaining to the first and the second exothermic peaks. As seen in Fig. 7a and b, parameters measured in four different non-isothermal DTA analysis provide approximately a linear fit of data points and the slope is nothing but Q/R (where $R = 8.31$ J/K mol, gas constant). The activation energy, Q can

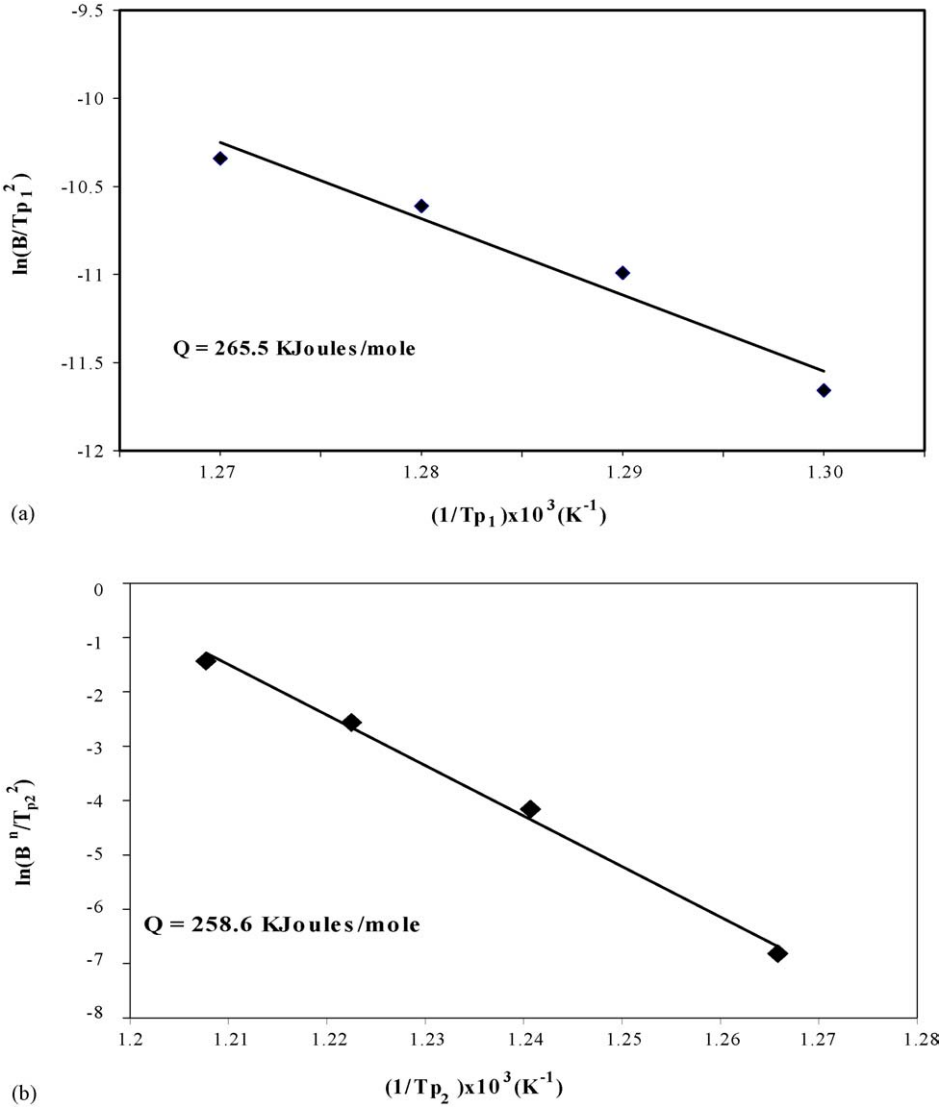

Fig. 7. (a) The modified Kissinger plot pertaining to the first exotherm (T_{p1}) of the $85TeO_2$–$15WO_3$ glass (Avrami parameter: $n = 1.2$ and the dimensionality of the crystal growth: $m = 1$). (b) The modified Kissinger plot pertaining to the second exotherm (T_{p2}) of the $85TeO_2$–$15WO_3$ glass (Avrami parameter: $n = 3.9$ and the dimensionality of the crystal growth: $m = 3$).

Table 3
Values of n and m for different crystallization mechanisms in the heating process[19,20,22]

Crystallization mechanism	n	m
Bulk crystallization with a constant number of nuclei (i.e., the number of nuclei is independent of the heating rate)		
Three-dimensional growth of crystals	3	3
Two-dimensional growth of crystals	2	2
One-dimensional growth of crystals	1	1
Bulk crystallization with an increasing number of nuclei (i.e., the number of nuclei is inversely proportional to the heating rate)		
Three-dimensional growth of crystals	4	3
Two-dimensional growth of crystals	3	2
One-dimensional growth of crystals	2	1
Surface crystallization	1	1

then be calculated as 265.5 kJ/mol associated with the first exothermic transformation and 258.6 kJ/mol associated with the second exothermic transformation. These values are comparable with the activation energy value of 238 kJ/mol for surface crystallization of paratellurite (α-TeO_2) crystals in a $0.7TeO_2$–$0.3LiCl$ glass.[7]

4. Conclusions

On the basis of the results reported in the present investigation, the following conlusions can be drawn:

1. The hypereutectic $0.7TeO_2$–$0.3WO_3$ and $0.75TeO_2$–$0.25WO_3$ glasses doped with 1 mol% Tm_2O_3 do not crystallize. On the other hand, devitrification of the hypoeutectic $85TeO_2$–$15WO_3$ glasses doped with 1 mol% Tm_2O_3 takes place in the vicinity of 490 °C and 530 °C with the crystallization of the α-TeO_2, γ-TeO_2 and WO_3 phases detected in the sample heated to about 510 °C and the transformation of γ-TeO_2 to α-TeO_2 detected in the sample heated to about 550 °C.
2. SEM investigations of the $0.85TeO_2$–$0.15WO_3$ glass heated to 510 °C revealed the presence of TeO_2-rich centrosymmetric fan-like crystals (between 3 μm and 30 μm in size) and WO_3-rich globular particles (3–4 μm in size) existing in the amorphous glass matrix formed as a result of surface crystallization. On the other hand, SEM and cross-sectional SEM micrographs of the $0.85TeO_2$–$0.15WO_3$ glass sample heated to 550 °C revealed TeO_2-rich lamellear crystals in the shape of long rods between 5 μm and 30 μm in length penetrated into the bulk in various directions, indicating that massive bulk crystallization was the dominant mechanism.
3. The crystallization behaviour of the $0.85TeO_2$–$0.15WO_3$ glasses was investigated using DTA in non-isothermal conditions. Using the Ozawa equation, the Avrami constant (n) was calculated as 1.2 and 3.9 for the first and second exothermic peaks on the DTA plots, indicating that surface crystallization and bulk crystallization are associated with the first exotherm and the second exotherm, respectively. The activation energy of crystal growth for the $0.85TeO_2$–$0.15WO_3$ glasses were determined using the modified Kissinger equation. The activation energy values are 265.5 kJ/mol for surface crystallization (first exothermic peak) and 258.6 kJ/mol for bulk crystallization (second exothermic peak).

Acknowledgements

The authors wish to express their thanks to Ms. Nurten Dinçer for her help in recording the DTA curves and in carrying out the SEM investigations. One of the authors (S. Cenk) is grateful to the management of TUBITAK, National Research Institute of Electronics for their support towards her Ph.D. dissertation work.

References

1. Auzel, F., Upconversion and anti-stokes processes with f and d ions in solids. *Chem. Rev.*, 2004, **104**(1), 139–173.
2. El-Mallawany, A. H., *Tellurite Glasses Handbook*. CRC Press, London, 2002.
3. Sidkey, M. A. and Gaafar, M. S., Ultrasonic studies on network structure of ternary TeO_2–WO_3-K_2O glass system. *Physica B*, 2004, **348**, 46–55.
4. Wang, J. S., Vogel, E. M. and Snitzer, E., Tellurite glasses: a new candidate for fiber devices. *Opt. Mater.*, 1994, **3**, 187–203.
5. Kim, S. H. and Yoko, T., Nonlinear optical properties of TeO_2-based glasses: Mo_x–TeO_2 (M = Sc, Ti, V, Nb, Mo Ta and W) binary glasses. *J. Am. Ceram. Soc.*, 1995, **78**(4), 1061–1065.
6. Burger, H., Vogel, W. and Kozhukharov, V., IR transmission and properties of glasses in the tellurium oxide (TeO_2)-[R_nO_m, R_nX_m, $R_n(SO_4)_m$ $R_n(PO_3)_m$ and boron oxide] systems. *Infrared Phys.*, 1985, **25**(1/2), 395–409.
7. Öveçoğlu, M. L., Özen, G., Demirata, B. and Genç, A., Microstructural characterization and crystallization kinetics of $(1-x)TeO_2$–xLiCl (x = 0.6–0.4 mol) glasses. *J. Eur. Ceram. Soc.*, 2001, **21**(3), 177–183.
8. Özen, G., Denis, J.-P., Genotelle, M. and Pellé, F., Tm-Yb-Tm energy transfers effect of temperature on the fluorescence intensities in oxyfluoride-tellurite compounds. *J. Phys.: Condens. Matter*, 1995, **7**, 4325–4336.
9. Kosuge, T., Benino, Y., Dimitrov, V., Sato, R. and Komatsu, T., Thermal stability and heat capacity changes at glass transition in K_2O–WO_3–TeO_2 glasses. *J. Non-Cryst. Solids*, 1998, **242**, 154.
10. Sekiya, T., Mochida, N. and Ogawa, S., Structural study of WO_3–TeO_2 glasses. *J. Non-Cryst. Solids*, 1994, **176**, 105–115.
11. Blanchandin, S., Marchet, P. P., Thomas, P., Champarnaud-Mesjard, J. C., Frit, B. and Chagraoui, A. B., New investigation within the TeO_2–WO_3 system: phase equilibrium diagram and glass crystallization. *J. Mater. Sci.*, 1999, **34**, 4285–4292.
12. Cenk, S., Demirata, B., Öveçoğlu, M. L. and Özen, G., Thermal properties and optical transition probabilities of Tm^{3+} doped TeO_2–WO_3 glass. *Spectrochim. Acta Part A*, 2001, **57**, 2367–2372.
13. Özen, G., Aydınlı, A., Cenk, S. and Sennaroğlu, Effect of composition on the spontaneous emission probabilities, stimulated emission cross-sections and local environment of Tm^{3+} in TeO_2–WO_3 glass. *J. Lumin.*, 2003, **101**(4), 293–306.
14. Salje, E. and Viswanathan, K., Physical properties and phase transitions in WO_3. *Acta Cryst. A*, 1975, **A31**, 356–359.

15. Powder Diffraction File, Card no. 42-1365, 1992 Database Edition, Joint Committee on Powder Diffraction Standards (JCPDS), Swathmore, PA, USA.
16. Powder Diffraction File, Card no. 20-1324, 1992 Database Edition, Joint Committee on Powder Diffraction Standards (JCPDS), Swathmore, PA, USA.
17. Öztürk, A., Crystallization kinetics of fluorophosphate glasses: part I. Effect of composition and heating rate. *J. Mater. Sci.*, 1997, **32**, 2623–2627.
18. Ray, C. S., Yang, Q., Huang, W. and Day, D. E., Surface and internal crystallization in glasses as determined by differential thermal analysis. *J. Am. Ceram. Soc.*, 1996, **79**(12), 3155–3160.
19. Erol, M., Küçükbayrak, S., Ersoy-Meriçboyu, A. and Öveçoğlu, M. L., Crystallization behaviour of glasses produced from fly ash. *J. Eur. Ceram. Soc.*, 2001, **21**, 2835–2841.
20. Matusita, K., Sakka, S. and Matsui, Y., Determination of the activation energy for crystal growth by DTA. *J. Mater. Sci.*, 1975, **10**, 961–966.
21. Matusita, K. and Sakka, S., Kinetic study on cyrstallization of the glass by DTA-criterion on application of Kissinger plot. *J. Non. Cryst. Sol.*, 1980, **38-39**, 741–746.
22. Matusita, K. and Sakka, S., *Bull. Inst. Chem. Res. Kyoto Univ.*, 1981, **59**, 159.
23. Abel-Rahim, M. A., Ibrahim, M. M., Dongol, M. and Gaber, A., *J. Mater. Sci.*, 1992, **27**, 4685.
24. Kissinger, H. E., Variation of peak temperature with heating rate in differential thermal analysis. *Jr. Res. Nat. Bur. Stand.*, 1956, **57**, 217–221.
25. Ozawa, T., Kinetics of non-isothermal crystallization. *Polymer*, 1971, **12**, 150–158.